

Strong Evidence for an Unprecedented Borderline Case of Dissociation and Cycloaddition in Open-Shell 1,3-Dipole Chemistry: Transient Nitrilium Phosphane-Ylide Complex Radical Cations

Holger Helten,^[a] Stefan Fankel,^[a] Ovidiu Feier-Iova,^[b] Martin Nieger,^[c]
Arturo Espinosa Ferao,^{*[d]} and Rainer Streubel^{*[a]}

Keywords: Density functional calculations / Electron transfer / Single electron transfer reactions / Radical ions / HSAB parameters

The reaction of 3-ferrocenyl-substituted 2*H*-azaphosphirene complexes **1a–c** in the presence of substoichiometric amounts of ferrocenium hexafluorophosphate yields 3,5-diferrocenyl-substituted 2*H*-1,4,2-diazaphosphole complexes **3a–c** and difluoro(organo)phosphane complexes **4a–c**. The reaction of **1a,c** and [FcH]PF₆ with cyanoferrocene yields **3a,c** in a straightforward way. The molecular structures of **3a,c** were unambiguously identified by multinuclear NMR spectroscopic experiments, mass spectrometry, and single-crystal X-ray diffraction studies. DFT calculations on model complexes

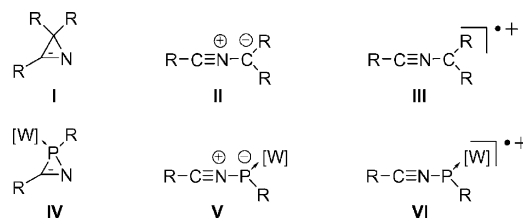
1d–m and **3d–m** reveal a close similarity of Mo and W complexes (vs. Cr) and a strong influence of the ferrocenyl substituent on the geometry, spin, and charge distribution of reactive intermediates and the reaction course. Strong support for the assumption of a dissociation–cycloaddition reaction sequence leading to **3** and thus a surprising “cannibalistic” reaction was obtained.

(© Wiley-VCH Verlag GmbH & Co. KGaA, 69451 Weinheim, Germany, 2009)

Introduction

It is long known that C–C bond cleavage of 2*H*-azirenes **I** by thermal^[1] or photochemical^[2] reaction yields transient nitrile ylides **II** (Scheme 1), which belong to the class of 1,3-dipoles and thus are very useful building blocks for the synthesis of N-heterocycles. More recent investigations have shown that photoinduced electron-transfer (PET) oxidation of 2*H*-azirenes causes formation of transient 2-azaallenyl radical cations **III** that, like their neutral counterparts, nitrile ylides **II**, react preferentially with electron-poor 2π systems to give the corresponding five-membered N-heterocycles.^[3] In comparison to their neutral analogs, these 2-azaallenyl radical cations exhibit enhanced reactivity, sometimes higher selectivity, and their reactions with dipolarophiles proceed through a two-step mechanism. Recently, Mattay

reported SET oxidations of aziridines to form transient azomethine ylide radical cations^[4] that can yield five-membered heterocycles as final products, thus behaving as open-shell 1,3-dipoles.



Scheme 1. 2*H*-Azirenes (**I**), nitrile ylides (**II**), nitrile ylide radical cations (2-azaallenyl radical cations) (**III**), 2*H*-azaphosphirene complexes (**IV**), nitrilium phosphane-ylide complexes (**V**) and nitrilium phosphane-ylide complex radical cations (**VI**) ([W] = W(CO)₅; R denotes an organic substituent).

As often seen in the chemistry of phosphoorganic compounds that have a low-coordinate phosphorus center such as phosphalkenes or phosphabenzenes (phosphinines), the diagonal relationship of phosphorus and carbon is striking, albeit some differences in bonding and reactivity remain.^[5,6]

At the beginning of our work on 2*H*-azaphosphirene complexes **IV**^[7] (Scheme 1), we had also observed similarities to 2*H*-azirenes **I**, as complexes **IV** form nitrilium phosphane-ylide complexes **V**^[8] upon heating or irradiation; lately, these species became very valuable building blocks in P-heterocycle synthesis. Some years ago, we became inter-

[a] Institut für Anorganische Chemie, Rheinische Friedrich-Wilhelms-Universität Bonn, Gerhard-Domagk-Str. 1, 53121 Bonn, Germany
Fax: +49-228-73-9616
E-mail: r.streubel@uni-bonn.de

[b] Institut für Anorganische Chemie, Ruprecht-Karls-Universität Heidelberg, Im Neuenheimer Feld 270, 69120 Heidelberg, Germany

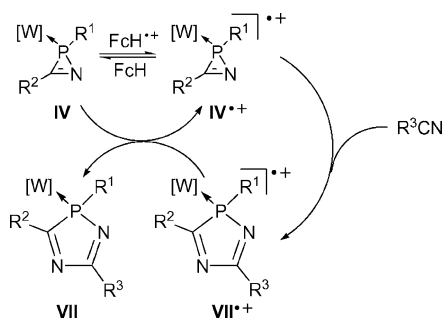
[c] Laboratory of Inorganic Chemistry, Department of Chemistry, University of Helsinki,

P. O. Box 55 (A. I. Virtasen aukio 1), 00014 Helsinki, Finland
[d] Departamento de Química Orgánica, Facultad de Química, Campus de Espinardo, Universidad de Murcia, 30100 Murcia, Spain

Supporting information for this article is available on the WWW under <http://dx.doi.org/10.1002/ejic.200900314>.

ested in exploring the reactivity of 2*H*-azaphosphirene tungsten complexes towards SET oxidants such as ferrocenium hexafluorophosphate.^[9]

Under these conditions, complexes **IV** exhibit a ligand-centered reactivity,^[10] i.e., they undergo P–N bond-selective ring expansion to give eventually complexes **VII** in a radical chain reaction if at least 0.03 equiv. ferrocenium salt is employed (Scheme 2). Thorough DFT calculations provide further support for transiently formed nitrilium phosphane-ylide tungsten complex radical cations **VI** (Scheme 1).^[11] As part of our current research is focused on template-directed synthesis of functional heterocycles, we recently conducted oxidative SET reactions of 3-ferrocenyl-substituted 2*H*-azaphosphirene tungsten complexes with electron-rich nitrile derivatives by using ferrocenium hexafluorophosphate.^[12] Some of these reactions showed a nitrile-dependent degree of byproduct formation, whereas the latter displayed ³¹P{¹H} NMR spectroscopic data typical for a 2*H*-1,4,2-diazaphosphole complex but with an unknown substitution pattern.^[12] As this ring expansion methodology offers the interesting perspective to construct extended ligand architectures with redox-active functionalities, it became a necessity to understand and thus be able to disfavor or avoid this side reaction.



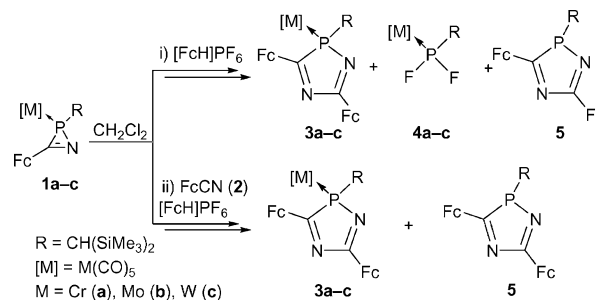
Scheme 2. Proposed catalytic cycle of the ferrocenium-salt-induced ring expansion of 2*H*-azaphosphirene complexes ([W] = W(CO)₅; R¹–R³ denote organic substituents).

Here we present first results of transient nitrilium phosphane-ylide complex radical cation dissociation and 1,3-dipole reactions that represent an unprecedented borderline case in open-shell 1,3-dipole chemistry. The combined experimental and theoretical study addresses ligand, nitrile, as well as metal effects on stability and reactivity of these unusual open-shell reactive intermediates (**VI**).

Results and Discussion

We first performed reactions by using tungsten complexes, because highly valuable information about reaction products can be gained from ³¹P{¹H} NMR satellite spectra, which facilitates reaction control. The reaction of 3-ferrocenyl-substituted 2*H*-azaphosphirene complex **1c**^[12] in the presence of substoichiometric amounts of ferrocenium hexafluorophosphate but in the *absence* of a nitrile yielded the 3,5-diferrocenyl-substituted 2*H*-1,4,2-diazaphosphole complex **3c** at ambient temperature (Scheme 3, i). To our

surprise, difluorophosphane complex **4c**^[13] was formed, too, which complicated the workup.^[14] Therefore, the reaction of **1c** and [FcH]PF₆ was repeated in the presence of 1 equiv. cyanoferrocene (FcCN) (**2**), which yielded **3c** in a clean reaction (Scheme 3, ii). The molecular structure of **3c** was unambiguously confirmed by multinuclear NMR spectroscopic experiments, mass spectrometry, and a single-crystal X-ray diffraction study (Figure 1).^[15]



Scheme 3. Reactions of 2*H*-azaphosphirene complexes **1a–c** in the presence of ferrocenium hexafluorophosphate in the *absence* (i) or *presence* (ii) of FcCN.

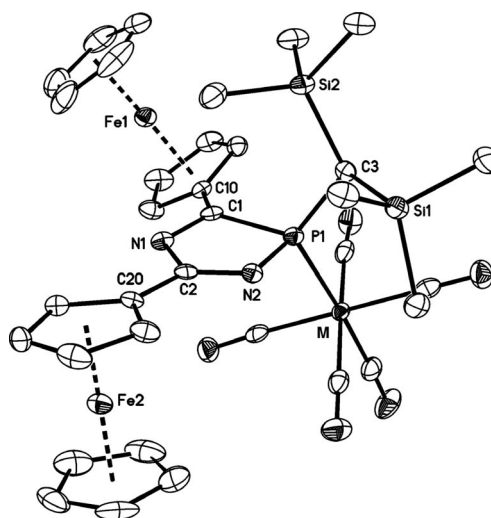


Figure 1. Molecular structure of complex **3a** (M = Cr) in the crystal (50% probability level, hydrogen atoms are omitted for clarity). Selected bond lengths in Å and angles in °: Cr1–P1 2.4047(6), P1–C3 1.830(2), P1–N2 1.6920(17), P1–C1 1.880(2), C1–N1 1.304(3), N1–C2 1.432(3), C2–N2 1.294(2), C2–C20 1.455(3), C1–C10 1.460(3); N2–P1–C1 90.37(9), P1–C1–N1 108.81(16), C1–N1–C2 109.97(17), N1–C2–N2 120.44(19), C2–N2–P1 109.57(15), P1–C1–C10 128.33(16), N2–C2–C20 117.03(18). For isotopic complex **3c** (M = W): W1–P1 2.5283(10), P1–C3 1.824(4), P1–N2 1.697(3), P1–C1 1.882(3), C1–N1 1.299(4), N1–C2 1.423(5), C2–N2 1.301(4), C2–C20 1.451(5), C1–C10 1.464(5); N2–P1–C1 90.40(15), P1–C1–N1 108.6(3), C1–N1–C2 110.5(3), N1–C2–N2 120.4(3), C2–N2–P1 109.2(3), P1–C1–C10 128.2(3), N2–C2–C20 121.9(3).

In order to study the dependence of the unexpected reaction (i) on the nature of the pentacarbonyl metal fragment, we also reacted the chromium and molybdenum complexes **1a,b**, which were easily obtained by using the synthetic protocol for complex **1c**,^[12] with [FcH]PF₆ under analogous conditions in the *absence* (i) and in the *presence* (ii) of cyanoferrocene (**2**). During reaction (i) of complex **1b**, reso-

nances at $\delta = 132.6$ and 96.3 ppm were detected by $^{31}\text{P}\{^1\text{H}\}$ NMR spectroscopy, which are tentatively assigned to complex **3b** and the liberated heterocyclic ligand **5**, respectively.^[17] In the reaction of chromium complex **1a** (i) the formation of **3a** was observed. Both reactions also yielded difluorophosphane complexes **4a**^[13] and **4b**^[13] as byproducts that were identified on the basis of their typical NMR spectroscopic parameters. In the chromium case, a clean reaction was also achieved if FcCN was added (ii). The molecular structure of **3a** was unambiguously determined by multinuclear NMR spectroscopic experiments, mass spectrometry, and a single-crystal X-ray diffraction study (Figure 1).^[15]

Within the series of metal complexes **3a–c** the $^{31}\text{P}\{^1\text{H}\}$ NMR spectra show a typical upfield shift of the ^{31}P resonance upon going from Cr (**a**) to Mo (**b**) and W (**c**), which is a common feature of coordinated trivalent phosphorus compounds^[19] (Table 1). On the other hand, the $^{13}\text{C}\{^1\text{H}\}$ NMR spectroscopic data of the ring carbons are almost unaffected by changing the group 6 metal. The C^3 resonances are strongly deshielded, especially in comparison to the values of the C^5 carbon centers. Furthermore, the sum of the scalar phosphorus–carbon couplings reveal some self-canceling effects in the case of $^{2+3}J(\text{P,C})$ couplings, whereas the magnitudes for $^{1+4}J(\text{P,C})$ couplings of **3a,c** are significantly larger.

Table 1. $^{31}\text{P}\{^1\text{H}\}$ and $^{13}\text{C}\{^1\text{H}\}$ NMR spectroscopic data of complexes **3a–c**.^[18]

	3a ^[a]	3b ^[b]	3c ^[a]
δ_{P} /ppm	158.1	132.6	113.4
$^1J(\text{W,P})$ /Hz	—	—	234.0
$\delta_{\text{C}}(\text{C}^3)$ /ppm	205.3 ^[c]	[d]	206.6
$^{1+4}J(\text{P,C})$ /Hz	12.0 ^[c]	[d]	27.5
$\delta_{\text{C}}(\text{C}^5)$ /ppm	171.6 ^[c]	[d]	175.1
$^{2+3}J(\text{P,C})$ /Hz	6.8 ^[c]	[d]	5.8

[a] In C_6D_6 . [b] In CH_2Cl_2 . [c] In CDCl_3 . [d] Not determined.

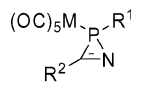
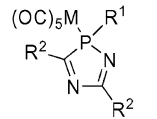
The solid-state structures of complexes **3a** and **3c** are isotopic; they feature localized C–N double bonds of around 1.30 \AA , a long endocyclic P–C bond of approximately 1.88 \AA , a long coordinative P–M bond [$2.4047(6)$ and $2.5283(10) \text{ \AA}$], and a narrow endocyclic angle at phosphorus [$90.37(9)$ and $90.40(15)^\circ$]. The largest endocyclic bond angle is found at C2 as apex [$120.44(19)$ and $120.4(3)^\circ$]. Notwithstanding the presence of two bulky ferrocenyl substituents, the phosphorus heterocycles are largely planar (mean deviations from least-squares planes: 0.065 and 0.067 \AA). With respect to each other, the ferrocenyl moieties exhibit a *transoid* orientation at the heterocycle.

The cyclopentadienyl ring at C2 [at the Fe2 ferrocenyl unit] adopts a coplanar arrangement with respect to the heterocycle (torsion angles of the ring planes with respect to least-squares planes: 7.75 and 6.86°). In contrast, the Cp ring of the ferrocenyl unit at C1 [at the Fe1 ferrocenyl unit] is out of the heterocycle ring plane and the Cp ring at C1 subtends an interplanar angle of 31.85° (**3a**) and 31.82°

(**3c**). The reason for this distortion is presumably the proximity to the bulky bis(trimethylsilyl)methyl group, which gives rise to strong steric repulsion.

Theoretical Approach

Ring expansion pathways were evaluated by means of DFT methods (see below). The stationary points for several conceivable paths were thoroughly checked for the simplest *2H*-azaphosphirene complex derivatives **1d–f**, i.e., having methyl groups for R^2 (Scheme 4). Unless otherwise stated, a methyl group was used as the R^1 substituent at phosphorus for the sake of simplicity (entries d–l). The selected lower energy paths were then explored for other *P*- (R^1) and *C*-substituents (R^2). The influence of the solvent (dichloromethane) was taken into account by means of single-point calculations with Cossi and Barone's CPCM (conductor-like polarizable continuum model) modification^[20] of Tomasi's PCM formalism,^[21] performed on the gas-phase geometries.

	entry	R^1	R^2	M
 1	d	Me	Me	Cr
	e	Me	Me	Mo
	f	Me	Me	W
	g	Me	Ph	Cr
 3	h	Me	Ph	Mo
	i	Me	Ph	W
	j	Me	Fc	Cr
	k	Me	Fc	Mo
	l	Me	Fc	W
	m	$\text{CH}(\text{SiH}_3)_2$	Me	W

Scheme 4. Calculated model complexes **1d–m** and **3d–m**.

First, the energetics of the SET steps were evaluated, according to Equations (1), (2), and (3).



Equations (1) and (2) represent the ease of oxidation of the *2H*-azaphosphirene and *2H*-1,4,2-diazaphosphole complexes by reaction with the ferrocenium cation; (1) corresponds to the initiator step of the chain reaction (cf. Scheme 2). Equation (3), resulting from the difference (1) – (2), is the final step yielding the neutral product **3** with reformation of the species $\mathbf{1}^{+\bullet}$. The values of ΔG° for these reactions are plotted in Figure 2, from which two important conclusions can be drawn. First, similar values are obtained for the methyl and phenyl derivatives, both reactions (1) and (2) being endergonic and the final step of the cycle (3) being moderately exergonic. For ferrocenyl derivatives, the situation is reversed, as both (1) and (2) are exergonic but not (3), which is slightly endergonic. Second, regarding the pentacarbonyl metal fragment, in the cases of the methyl and phenyl derivatives, remarkable similarities are observed for Mo and W in comparison to Cr and the easiness for the final redox step varies in the order $\text{Cr} < \text{Mo} \leq \text{W}$.^[22] This

is also in line with the common trend of redox potentials for complexes of the general formula $[M(CO)_5(PR_3)]$, which usually shows the relationship $Cr < Mo < W$.^[23]

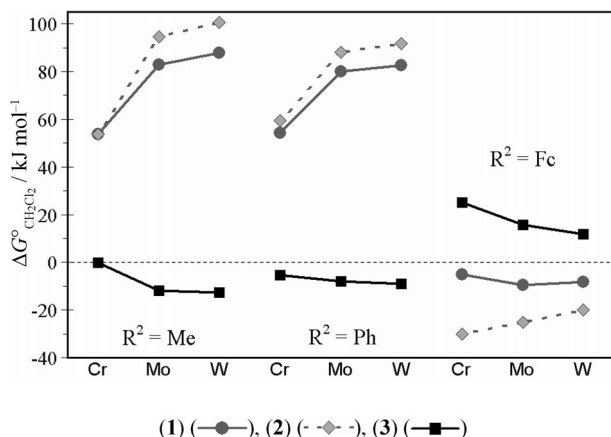


Figure 2. Variation of the Gibbs free energy corresponding to processes displayed in Equations (1)–(3) upon changing the R^2 group and the metal, taking dichloromethane into account.

Moreover, the similarities found between Mo and W complexes and their differences from the Cr complexes were also observed in the variation of geometrical parameters upon oxidation. In Figure 3, percent increments in selected bond lengths are displayed, which will be discussed hereafter. Several conclusions regarding the effects of oxidation on the bonding in 1^{+} (Figure 3) and 3^{+} (see Supporting Information) seem to be apparent. Derivatives $1d-i^{+}$ ($R^2 = Me$ or Ph) show significant increases in the metal to the *trans*-carbonyl carbon bond lengths, which are largest for the Cr complexes. Although the P–M bond is affected less, these changes come together with a relative P–C ring bond lengthening, which is more pronounced for the Mo and W than for the Cr complexes, whereas the effect on the P–N ring bond is rather small (below $\pm 0.8\%$; not displayed). In total, the results point to a metal-centered oxidation, which therefore affects mostly the metal-to-ligand bonds, and thus the lengthening might be interpreted as reduced $M \rightarrow L$ π -backbonding. This is further supported by the observation of a C–O bond shortening of the *trans*-carbonyl ligand through oxidation (not displayed). The above-mentioned similarity between molybdenum and tungsten complexes upon oxidation was checked and was confirmed as a general trend by means of calculations performed on a series of oxidation reactions of common, acyclic phosphane complexes (see Supporting Information).

On the contrary, the ferrocenyl-substituted 2*H*-azaphosphirene complex derivatives $1j-i^{+}$ exhibited only small alterations of the geometric parameters related to the environment of phosphorus and the pentacarbonyl metal centers (most of them below $\pm 1\%$). This observation points to the fact that oxidation preferably occurred at the ferrocenyl moiety, which is further supported through the high positive charge and spin density located on the ferrocenyl group (see below). Geometrically significant for this group is the distance between the Fe center and the centroids of the cy-

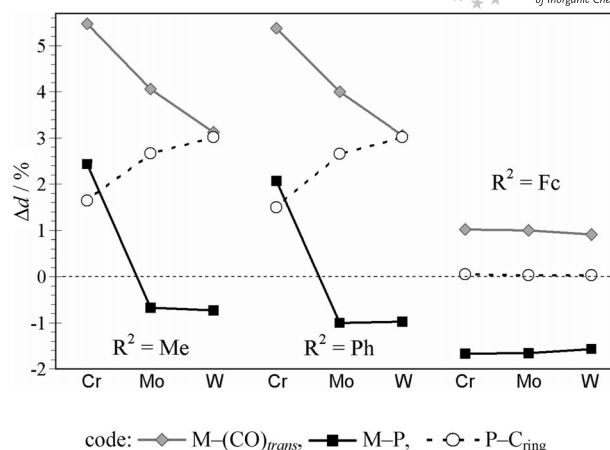


Figure 3. Effects of the substituent (R^2) and metal on the geometric changes of selected bonds upon oxidation of **1**.

clopentadienyl rings. It has previously been shown^[24] that this distance is of diagnostic relevance for characterizing the degree of oxidation in ferrocene or ruthenocene complexes, as it is almost insensitive to the nature of electron-donating or electron-withdrawing substituents but is considerably increased in radical cation metallocenium species, probably because of the removal of an electron that has slightly bonding character with respect to the metal Cp ring interaction. Thus, both $Fe-Cp^a$ and $Fe-Cp^b$ centroid distances^[25] are considerably elongated in $1j-i^{+}$ (Figure 4).

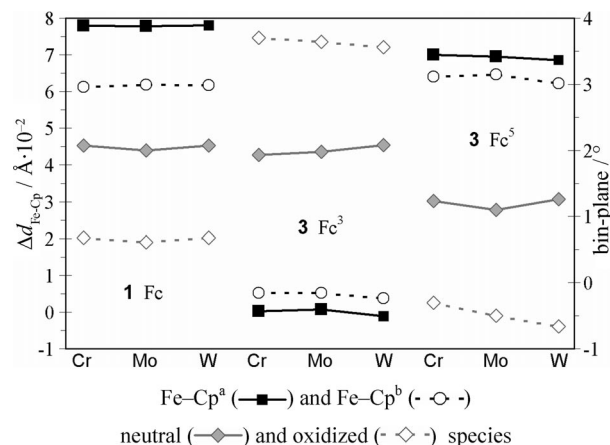


Figure 4. Relevant geometrical distortion parameters on oxidation for ferrocenyl groups in **1j-I** and **3j-I** (Fc^5 and Fc^3 ; see above): change in the $Fe-Cp^a$ and $Fe-Cp^b$ distances (in $\text{\AA} \cdot 10^{-2}$; y axis on the left) and $\beta_{in-plane}$ tilt angles in neutral and oxidized species (in $^\circ$; y axis on the right).

The picture of changes occurring for complex 3^{+} is more complicated, as a different behavior is observed for every substituent. In contrast to methyl and phenyl derivatives $3g-i^{+}$, their ferrocenyl counterparts $3j-i^{+}$ exhibit significantly small geometrical changes at both the heterocyclic ring and the metal carbonyl center, which are furthermore almost insensitive to changes in the nature of M .

The ferrocenyl group attached to C^5 of the diazaphosphole ring (Fc^5) experiences similar geometrical distortions to those of the Fc group in **1j-I**, which indicates that in the

oxidized species $3j\text{-I}^{+}$ the radical center is localized at Fc^5 , whereas the other ferrocenyl substituent at C^3 (Fc^3) remains essentially unoxidized, as shown by the almost unaffected $\text{Fe-Cp}^{\text{a,b}}$ distances (Figure 4). As previously reported,^[26] such kinds of essentially neutral ferrocenyl units can participate in alleviating an electron deficiency at neighboring positions by folding the $\text{Cp}^{\text{a}}\text{-Fe-Cp}^{\text{b}}$ axis. High values for $\beta_{\text{in-plane}}$ angles (the supplementary angle of the $\text{Cp}^{\text{a}}\text{-Fe-Cp}^{\text{b}}$ angle, taking only the component in the plane formed by the Fe atom and the C^1 -centroid axis in the Cp^{a} ring) account for a tilting of the Fe d_{z^2} -type orbital, which is involved in the σ interaction with both the a_{1g} MO of the unsubstituted Cp^{b} unit and the LUMO (π^*) of the fulvene-like structure of Cp^{a} (including the exocyclic bond).^[26] This participation is clearly observed in Fc^3 of $3j\text{-I}^{+}$ by the increase in β , but not in the oxidized ferrocenyl moieties Fc^5 in $3j\text{-I}^{+}$ or Fc in $1j\text{-I}^{+}$, whose β values decrease.

Therefore, the changes in bond strengths upon oxidation of derivative **11** to give **11**⁺ ($\text{R} = \text{Fc}$, $\text{M} = \text{W}$) were closely inspected, thus serving as a good case in point for the molybdenum – and in part for the chromium – complexes. The oxidation promotes a significant weakening of the P–N bond as underlined by the calculated decrease of –6.3% in the Wiberg Bond Index (WBI) ($0.856 \rightarrow 0.803$), whereas only a small weakening of –2.2% is computed for the P–C bond (WBI $0.903 \rightarrow 0.883$) (Figure 5).

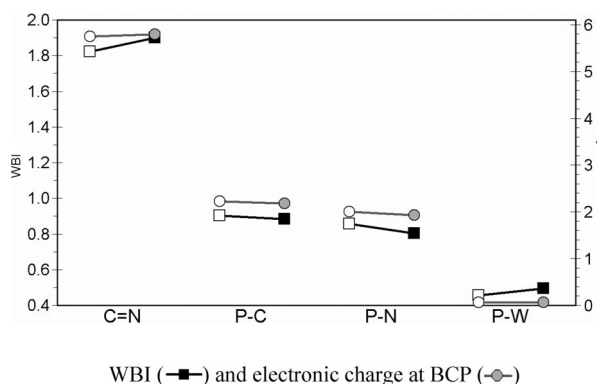
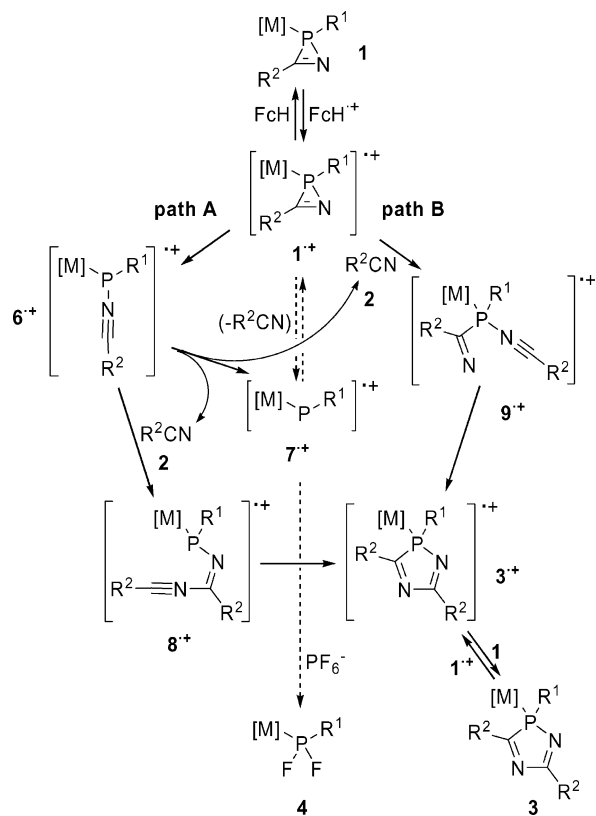


Figure 5. Changes in bond strengths upon oxidation $11 \rightarrow 11^{+}$ ($\text{R}^2 = \text{Fc}$, $\text{M} = \text{W}$): WBI and electronic charge at BCP (in $\text{e}\text{\AA}^{-3}$) between neutral (hollow squares or circles) and oxidized (filled squares or circles) species.

In addition, we turned to the atoms-in-molecules (AIM) methodology^[27] to get further insight, and here, Bader's topological analysis of the electronic charge density $\rho(r_c)$ revealed the same tendency inasmuch as, for the same metal and substituents, $\rho(r_c)$ at the respective bond critical points (BCP) is lower and decreases on oxidation more markedly for the P–N (–3.6%; $2.00 \times 10^{-2} \rightarrow 1.93 \times 10^{-2} \text{ e}\text{\AA}^{-3}$) than for the P–C bond (–2.1%; $2.23 \times 10^{-2} \rightarrow 2.18 \times 10^{-2} \text{ e}\text{\AA}^{-3}$)^[28] (Figure 5). According to their positive values of $\nabla^2\rho(r_c)$ both endocyclic bonds (P–C $0.95 \times 10^{-3} \rightarrow 3.01 \times 10^{-3} \text{ e}\text{\AA}^{-5}$, and P–N $4.90 \times 10^{-3} \rightarrow 4.03 \times 10^{-3} \text{ e}\text{\AA}^{-5}$) increase their ionic character,^[29] unlike the notably covalent C=N bond ($-3.15 \times 10^{-2} \rightarrow -2.96 \times 10^{-2} \text{ e}\text{\AA}^{-5}$) that is strengthened upon oxidation [$\rho(r_c) = 5.75 \times 10^{-2} \rightarrow$

$5.80 \times 10^{-2} \text{ e}\text{\AA}^{-5}$]. This feature points to an important contribution to the resonance hybrid in 1^{+} of a π -donor/ π -acceptor complex between a nitrile molecule **2** and a radical cationic phosphanylidene complex 7^{+} (Scheme 5), according to the Dewar–Chatt–Duncanson model.^[30] However, we did not find a path for the one-step dissociation of 1^{+} into 7^{+} and **2**. Despite the stronger character of the (endocyclic) P–C bond in comparison to the P–N bond, we found that the only feasible pathway for dissociation is a stepwise process starting with the initial breaking of the P–C bond to yield the radical cationic nitrilium phosphane-ylide complex 6^{+} that subsequently dissociates into complex 7^{+} (see below) and the nitrile **2**. The electronic distribution upon dissociation was checked twofold. First we performed a reaction coordinate study by stepwise elongation of the P–N bond in 6^{+} , which proved that the spin density remained almost exclusively on the phosphorus fragment. This finding was further supported by calculation of the thermochemical data corresponding to the couple **2** + 7^{+} in comparison to 2^{+} + **7** (Table 3).



Scheme 5. Calculated pathways for the transformation of 1^{+} into 3^{+} [$\text{M} = \text{M}(\text{CO})_5$; $\text{R}^1, \text{R}^2, \text{M}$: see Scheme 4].

The preference for the attack of **2** at the nitrilium C atom in 6^{+} to afford intermediate 8^{+} requires some detailed analysis, which was performed for the reaction of 6^{+} with FcCN . Pure electrostatic arguments based, for instance, on atomic natural charges^[31] would lead to a wrong prediction: N (0.944 au) > P (0.430 au) > C (–0.393 au). Mulliken charges would successfully point to C (0.547 au) as the preferred electrophilic site in comparison to N (–0.293 au) but

would not discriminate P (0.528 au). On the other hand, the Mulliken spin-density distribution depicted in Figure 6 provides evidence for a higher contribution of P over C and N atoms in the related β -LUMO (sum of absolute orbital coefficients 1.520, 0.538, and 0.336, respectively).^[32] Finally, steric crowding at phosphorus could be invoked together with electronic arguments in order to explain qualitatively the nucleophilic attack of the nitrile group at the carbon center in $6\mathbf{l}^+$.

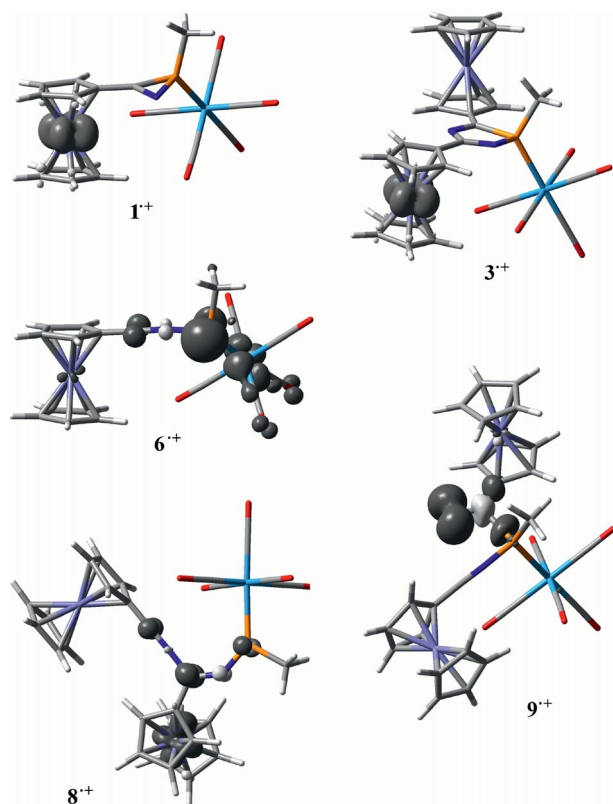


Figure 6. Calculated Mulliken spin density (isodensity 0.005 au) for $1\mathbf{l}^+$, $3\mathbf{l}^+$, $6\mathbf{l}^+$, $8\mathbf{l}^+$, and $9\mathbf{l}^+$ ($R^2 = \text{Fc}$; $M = \text{W}$).

Nevertheless, during the last two decades many important concepts and parameters related to chemical reactivity have been rationalized within the framework of DFT.^[33] The DFT formulation^[34] of Pearson's hard-soft acid-base (HSAB) principle^[35] states that the most favorable situation occurs when the reactants have equal softness provided that the charge reshuffling step can be neglected. The best suited *local* reactivity index for studying regioselectivity^[36] is local softness $s(r)$, easily obtained from the Fukui function $f(r)$, defined by Parr and Yang,^[37] and the global softness $S = (\partial N / \partial \mu)_{v(r)}$, which describes the ability of the molecule to take or lose electrons in response to a change in the chemical potential, μ . Therefore, $s(r)$ describes both the charge transfer between the reactants and how charge is redistributed within the reactants themselves. A local HSAB principle can then be devised as follows: a regioisomer is favored when the new bond is formed between atoms of equal softness. In other words, the preferred regioisomer in the reaction between atom k in molecule A and molecule B

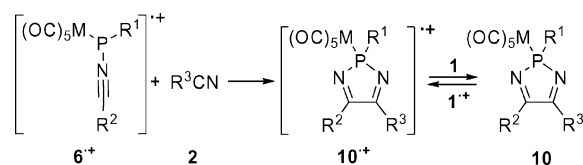
will be formed upon reaction at atom l that minimizes the quadratic difference in the local condensed-to-atom-softness function,^[38] $\Delta(s^2)_{kl} = (s_{Ak} - s_{Bl})^2$. An analogous parameter, $\Delta(\omega^2)_{kl} = (\omega_{Ak} - \omega_{Bl})^2$, has been proposed^[39] on the basis of local philicities $\omega(r)$, which, in turn, can be easily calculated – via Fukui functions $f(r)$ – from the global philicity,^[40] $\omega = \mu^2 S$, measuring the stabilization in energy when the system acquires an additional electronic charge, ΔN , from the environment. For situations in which condensed local softness was found inadequate for providing the correct intermolecular reactivity trends, the group softness,^[41] $s_{(k)g}$, and group philicity,^[42] $\omega_{(k)g}$, descriptors have been highlighted, which are obtained after summing the condensed local property – softness or philicity – over all of the n neighboring atoms attached to the reactive site k . Finally, in the very first step of the bond-forming interaction between atoms k and l , charge is transferred within them, equalizing the electron chemical potential and inducing a variation of the grand potential, $\Delta\Omega$, of the system. The contribution due to the interaction of atoms k and l is $\Delta\Omega_{kl} = -0.5(\mu_A - \mu_B)^2 s_{Ak} s_{Bl} / (s_{Ak} + s_{Bl})$. All three parameters, $\Delta(s^2)_{kl}$, $\Delta(\omega^2)_{kl}$, and $\Delta\Omega_{kl}$, calculated for the nucleophilic attack of FcCN to $6\mathbf{l}^+$ ($R^2 = \text{Fc}$, $M = \text{W}$), point to a more favorable reaction at the electrophilic C atom (Table 2) yielding intermediate $8\mathbf{l}^+$ that would rapidly cyclize to the oxidized diazaphosphole derivative $3\mathbf{l}^+$.

Table 2. Relevant HSAB-related calculated parameters^[a] for the reaction of $6\mathbf{l}^+$ ($R = \text{Fc}$, $M = \text{W}$) with FcCN.

	Nucleophilic attack			[3+2] Cycloaddition	
	C	N	P	P...C C...N	P...N C...C
$\Delta(s^2)_{kl}$	0.21	0.84	2.52	3.04 ^[d]	3.70 ^[d]
$\Delta(\omega^2)_{kl}$ ^[b]	0.25	0.49	2.20	3.27 ^[d]	3.38 ^[d]
$\Delta\Omega_{kl}$ ^[c]	9.4	128.8	11.5	3.4	4.6

[a] Derived from natural charges. [b] $\times 10^2$. [c] In kJ mol^{-1} . [d] Group properties.

Additionally, two regiochemically different [3+2] cycloaddition reactions between $6\mathbf{l}^+$ and nitriles 2 could be envisaged. One of them opens a path for the formation of isomeric 2*H*-1,3,2-diazaphosphole complexes 10 (Scheme 6). The two [3+2] cycloadditions can also be discriminated by means of an adapted set of DFT-HSAB parameters. For the case of the above-mentioned reaction between $6\mathbf{l}^+$ ($R^2 = \text{Fc}$, $M = \text{W}$) and FcCN, the same three parameters, $\Delta(s^2)_{kl}$, $\Delta(\omega^2)_{kl}$, and $\Delta\Omega_{kl}$, computed by summing up both interactions of P and C in $6\mathbf{l}^+$ with C and N in FcCN,



Scheme 6. [3+2] Cycloaddition pathway leading to isomers 10 (R^1 , R^2 , M : see Scheme 4).

predict a more favorable cycloaddition leading to **31**⁺ (Table 2), but the corresponding path has not been found in the potential energy surface at the working level of theory.

On the other hand, the mechanistic pathway leading to regioisomers **10** was found and thoroughly studied for R² = Me (M = Cr, Mo, W) (Figure 7). In spite of the fact that isomers **10d–f**⁺ are thermodynamically more stable than **3d–f**⁺ (as also are **10d–f** in relation to **3d–f**), their formation seems to be kinetically hampered by the relatively high energy barrier (Table 3) associated with their formation, in agreement with the HSAB-based results. Figure 7 shows the energy profiles for three selected representative examples

having R¹ = Me and M = W (R² = Me, Ph, Fc), which will be used for further discussions hereafter, unless otherwise stated.

Although no stable intermediates were found for the direct P–N bond cleavage of 2*H*-azaphosphirene radical cations **1**⁺, this ring-opening process can be achieved by nucleophilic addition of nitrile **2** (once formed from the dissociation of **6**⁺) at the phosphorus center of **1**⁺. This reaction proceeds by breaking of the weaker P–N bond and affords a new acyclic intermediate **9**⁺.^[43] Also cyclization of **9**⁺ to its valence isomer **3**⁺ proceeds through a very low-lying transition state (TS) that in some cases could not be

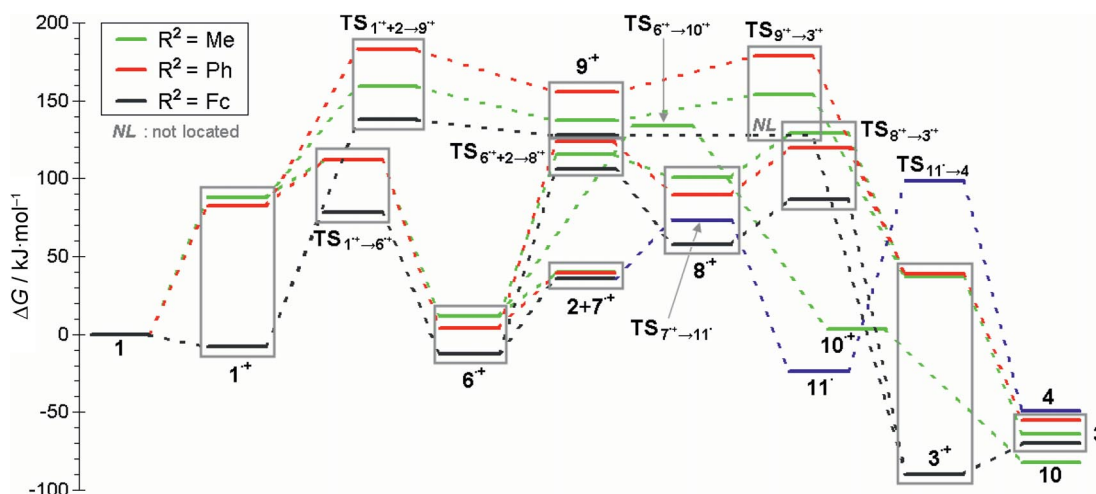


Figure 7. Calculated minimum energy paths (relative Gibbs free energy) for three selected examples [(R¹ = Me, M = W; R² = Me (green), Ph (red), or Fc (black))] and decomposition path of **7**⁺ leading to byproducts **4** (blue). Every step is appropriately counterbalanced both in matter (added reagents or lost units) and charge (by means of the FcH/FcH⁺ redox couple).

Table 3. Calculated thermochemical data^[a] for reactions depicted in Schemes 5, 6, and 7: ΔG° and ΔG(TS) (in parentheses).

Reaction	R ¹ R ² M	Me Me Cr	Mo Mo e	W W F	Ph Cr g	Mo Mo h	W W i	Fc Cr j	Mo Mo k	W W l	CH(SiH ₃) ₂ Me W m
1 → 1 ⁺ [b]		53.6	82.8	87.9	54.1	80.1	82.5	−7.2	−9.6	−8.2	78.9
1 ⁺ → 6 ⁺		(44.2)	(27.3)	(24.0)	(43.3)	(27.5)	(29.5)	(80.6)	(86.7)	(86.4)	(22.4)
6 ⁺ → 7 ⁺ + 2 [c]		−49.5	−76.2	−76.1	−54.2	−74.5	−78.7	−14.9	−4.4	−4.4	−75.7
6 ⁺ + 2 → 8 ⁺		32.4	34.9	28.2	40.3	37.5	35.4	57.2	51.0	48.5	5.6
		(107.6)	(110.5)	(103.9)	(124.9)	(118.7)	(119.9)	(129.6)	(119.8)	(118.5)	(103.4)
8 ⁺ → 3 ⁺		97.7	92.9	88.6	93.7	88.4	85.9	83.0	72.7	70.2	85.7
		(20.5)	(29.8)	(28.4)	(26.2)	(29.0)	(30.1)	(32.4)	(29.0)	(29.1)	(49.9)
3 ⁺ → 3 [b]		−105.5	−70.4	−63.7	−85.5	−59.4	−50.9	−156.8	−149.4	−147.5	−53.0
1 ⁺ + 2 → 9 ⁺		−53.8	−94.7	−100.6	−59.4	−88.1	−93.8	30.2	25.3	20.0	−98.0
		(100.8)	(76.2)	(71.6)	(124.0)	(105.3)	(100.4)	(139.5)	(151.6)	(145.9)	(73.0)
9 ⁺ → 3 ⁺		80.3	55.3	49.7	99.0	73.8	73.1	135.3	136.0	136.1	63.0
		[c]	(17.9)	(16.6)	[c]	(23.5)	(23.3)	[c]	[c]	[c]	(22.7)
2 + 7 ⁺ → 2 ⁺ + 7		−137.7	−109.0	−100.8	−147.9	119.3	−116.8	−223.9	−217.1	−217.7	−106.0
6 ⁺ + 2 → 10 ⁺		394.8	392.0	384.2	184.2	181.4	173.6	45.1	42.3	34.5	383.8
		(122.9)	(125.4)	(121.7)	[d]	[d]	[d]	[d]	[d]	[d]	(134.9)
10 ⁺ → 10 [b]		−30.4	−7.5	−8.8							5.2
7 ⁺ + PF ₆ [−] → 11 ⁺ + PF ₅		−65.4	−85.9	−85.1	[d]	[d]	[d]	[d]	[d]	[d]	−93.6
		(41.7)	(37.3)	(37.1)							(49.4)
11 ⁺ + PF ₅ → 4 + PF ₄ ⁺		−59.4	−60.9	−60.0							−40.6
		(122.2)	(121.0)	(122.4)							(132.3)
		−26.2	−25.7	−25.4							−20.9

[a] In kJ mol^{−1}. [b] Counterbalanced with the FcH/FcH⁺ redox pair, TS not calculated. [c] TS not located. [d] Not calculated.

located. Thermochemical data for all involved processes are collected in Table 3. The most relevant features can be summarized as follows: When the 2*H*-azaphosphirene ring substituent R^2 is methyl or phenyl, the displayed behavior is quite similar. Replacement by ferrocenyl promotes significant changes, mainly due to the relatively strong stabilization of the oxidized forms of $1j-I^+$ and the final products $3j-I^+$ as discussed above (see Figure 2). As already underlined before, molybdenum and tungsten complexes display large similarities, whereas chromium complexes show remarkable differences.

For $R^2 = \text{Me}$, once $1f$ is oxidized, ring opening proceeds easily to afford $6f^+$ (path A), from which a molecule of nitrile 2 is released through an endergonic dissociative process. The nitrile molecule MeCN can then react with $6f^+$ to give $8f^+$, but the required energetic barrier ($103.9 \text{ kJ mol}^{-1}$) is significantly higher than that needed for the reaction with $1f^+$ leading to $9f^+$ (71.6 kJ mol^{-1}) (path B). This step is then followed by an almost barrierless process to afford $3f^+$. Therefore, in the case of $R^2 = \text{Me}$, path A is only required as a source of nitrile 2 but is not further followed in the way to final product $3f$.

Furthermore, for $R^2 = \text{Me}$ and $M = W$ (as a good case in point), we have studied the effect of replacing the *P*-substituent (R^1) by the more sterically demanding $\text{CH}(\text{SiH}_3)_2$ group, which is close to the real system. With the exception of a more facile oxidation of $1m$ and the scarcely endergonic character of the dissociation into 7^+ and 2 , there are no remarkable differences, especially with regard to the activation energy of key steps leading to $8m^+$ ($103.4 \text{ kJ mol}^{-1}$) and $9m^+$ (73.0 kJ mol^{-1}). The same holds on moving from a methyl to a phenyl group as ring substituent R^2 : the activation energy for the formation of intermediate $8i^+$ ($119.9 \text{ kJ mol}^{-1}$) is higher than that associated with $9i^+$ ($100.4 \text{ kJ mol}^{-1}$).

Conversely, the ferrocenyl-substituted derivative maintains a similar value for the energetic barrier in the nucleophilic attack of FcCN to $6l^+$ ($118.5 \text{ kJ mol}^{-1}$), but undergoes a large increase in the activation energy corresponding to the nitrile-promoted 2*H*-azaphosphirene ring opening to yield $9l^+$ ($145.9 \text{ kJ mol}^{-1}$). So, in this case, path B is kinetically disfavored, and path A works not only as a source for the (required) free nitrile but also affords the electrophilic species $6l^+$ as precursor for the open-chain intermediate $8l^+$.

The origin for such a dramatic change in the preferred mechanistic pathway can be mainly attributed to the very different extent to which the ferrocenyl groups affect the stability of the involved intermediates. Inspection of Figure 7 revealed that all Fc-containing cationic species are slightly stabilized by comparison with the Me- or Ph-substituted derivatives, excepting the first oxidized species $1j-I^+$ and the very last one, $3j-I^+$, that are stabilized to a large extent. The reason should be the different stabilization of the unpaired electron and the positive charge.

Figure 8 represents the variation of the Mulliken spin density and natural charge along the critical path A in the proposed mechanistic scheme, and summed up for all atoms

forming every one of the selected four fragments; please note that R^3 and R^5 stand for the R^2 substituents that are linked to positions C^3 and/or C^5 in the final product 3^+ . For both $R^2 = \text{Me}$ or Ph, following path A, the higher spin density starts (in 1^+) by being located on the metal fragment, thereafter (in 6^+ and 8^+) it is sequentially spread onto the P atom and the originally present $R^3\text{CN}$ fragment, and finally (in 3^+) it moves back to the metal center. The positive charge remains mainly on the P atom with important contributions of the metal center at the beginning (in 1^+) and the end (in 3^+) of the path. However, by ferrocenyl substitution, a significant amount of spin density is shifted to the Fc group at the $R^3\text{CN}$ fragment (see also Figure 6) both in $1l^+$ and $3l^+$ as well as – partially – in intermediate $8l^+$, but has almost no effect in delocalizing the spin density in the radical cationic nitrilium phosphane-ylide complex $6l^+$ or in $9l^+$ (see Figure 6). This selective Fc-mediated spreading of the unpaired electron – and hence stabilization – of $1l^+$ in relation to $9l^+$ hampers the formation of $9l^+$ through path B, and therefore indirectly favors path A, in which $8l^+$ shows enhanced stability through Fc dispersion of the unpaired charge density in relation to $6l^+$.

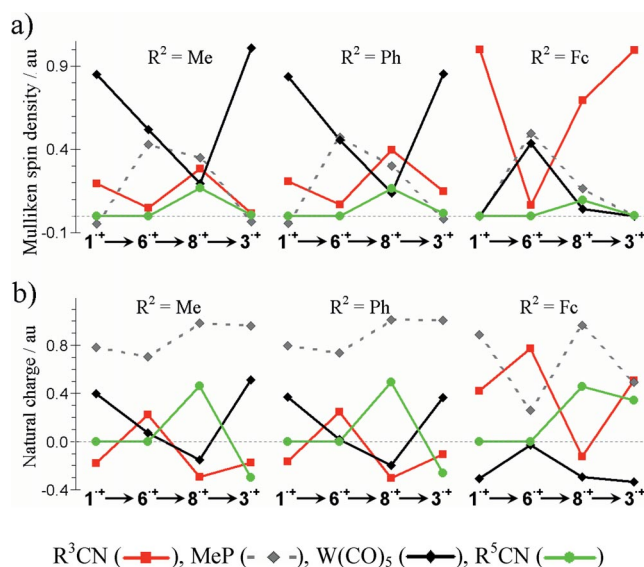
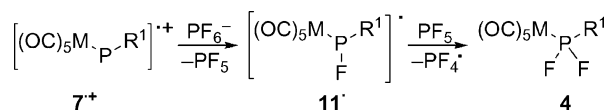


Figure 8. Changes in calculated Mulliken spin density (a) and natural charge (b) from $1f.i.l^+$ to $3f.i.l^+$ ($R^1 = \text{Me}$, $M = W$) in four selected fragments, $R^3\text{CN}$, MeP, $W(\text{CO})_5$, and $R^5\text{CN}$, along the mechanistic path A.

Finally, the endergonic character of the formation of 7^+ and nitrile 2 is largely compensated by the very exergonic (combined) reactions with PF_6^- leading to byproducts 4 (Table 3). Presumably this reaction proceeds by two sequential fluorination steps via radical intermediate 11^+ (Scheme 7).^[44]



Scheme 7. Proposed path for the formation of byproducts 4 (R^1 , M: see Scheme 4).

Conclusions

We have demonstrated that 3-ferrocenyl-substituted 2*H*-azaphosphirene complexes **1a–c** undergo a surprising reaction with ferrocenium hexafluorophosphate to yield 3,5-diferrocenyl substituted 2*H*-1,4,2-diazaphosphole complexes **3a–c** – in the absence of a nitrile – and difluoro(organo) phosphane complexes **4a–c**. According to DFT studies the symmetrically substituted 2*H*-1,4,2-diazaphosphole complexes are formed upon SET oxidation of complexes **1a–c**, which undergo a two-step dissociation via the radical cationic nitrilium phosphane-ylide complex **6⁺** that subsequently affords phosphanylidene complex **7⁺** and cyanoferrocene. Alternatively, **6⁺** can undergo stepwise cycloaddition with the latter to furnish finally the five-membered ring system according to the favored path A. The overall cycle of this SET-induced reaction is characterized not only by a close similarity of the transiently formed open-shell Mo and W complexes (vs. Cr) but by a strong influence of the ferrocenyl substituent (in contrast to methyl and phenyl) that dominates the spin and charge distribution of reactive intermediates and thus the reaction course. In total and to the best of our knowledge, this example represents an unprecedented borderline case of dissociation and cycloaddition in open-shell 1,3-dipole chemistry.

Experimental Section

General Procedures: All operations were performed in an atmosphere of deoxygenated and dried argon by using standard Schlenk techniques with conventional glassware. Solvents were distilled from sodium or CaH₂ (CH₂Cl₂). 2*H*-Azaphosphirene complexes **1a–c**^[12] and cyanoferrocene^[45] were synthesized according to the methods described in the literature. Melting points were determined with a Büchi apparatus Type S. The values are not corrected. NMR spectroscopic data were recorded with a Bruker Avance 300 spectrometer (¹H: 300.13 MHz; ¹³C: 75.5 MHz; ²⁹Si: 59.6 MHz; ³¹P: 121.5 MHz) at 30 °C by using C₆D₆ as solvent and internal secondary standard; shifts are referenced to tetramethylsilane (¹H; ¹³C; ²⁹Si, δ = 19.867187 MHz) and 85% H₃PO₄ (³¹P, δ = 40.480742 MHz). Mass spectra were recorded with a Kratos Concept 1H (FAB+, *m*NBA) or a MAT 95 XL Finnigan (EI, 70 eV, ¹⁸⁴W) spectrometer (selected data given). UV/Vis spectra were recorded with a Shimadzu UV-1650 PC spectrometer. Infrared spectra were recorded with a Thermo Nicolet 380 FTIR spectrometer (selected data given). Elemental analyses were performed by using an Elementar VarioEL instrument.

[[2-Bis(trimethylsilyl)methyl]-3-ferrocenyl-2*H*-azaphosphirene-κP]-pentacarbonylchromium(0)] (1a**):** Red solid; yield 0.39 g (0.66 mmol, 18%); m.p. 109 °C. ¹H NMR (C₆D₆): δ = 0.05 [s, 9 H, Si(CH₃)₃], 0.16 [s, 9 H, Si(CH₃)₃], 0.49 [d, ²*J*(P,H) = 3.3 Hz, 1 H, CH], 4.00 (s, 5 H, Fc-Cp^bH), 4.12 (m_c, 1 H, Fc-Cp^aH³), 4.15 (m_c, 1 H, Fc-Cp^aH⁴), 4.63 (m_c, 1 H, Fc-Cp^aH²), 4.88 (m_c, 2 H, Fc-Cp^aH⁵) ppm. ¹³C{¹H} NMR (C₆D₆): δ = −0.1 [d, ³*J*(P,C) = 3.6 Hz, Si(CH₃)₃], 0.8 [d, ³*J*(P,C) = 2.6 Hz, Si(CH₃)₃], 28.3 [d, ¹*J*(P,C) = 29.4 Hz, CH], 68.3 [d, ²*J*(P,C) = 17.5 Hz, Fc-Cp^aC¹], 68.8 [d, ³*J*(P,C) = 1.6 Hz, Fc-Cp^aC²H], 69.2 (s, Fc-Cp^bCH), 69.7 (s, Fc-Cp^aC³H), 71.1 (s, Fc-Cp^aC⁴H), 71.7 (s, Fc-Cp^aC⁵H), 191.5 (s, P-C=N), 215.1 [d, ²*J*(P,C) = 17.5 Hz, CO_{cis}], 218.6 [d, ²*J*(P,C) = 4.8 Hz, CO_{trans}] ppm; ³¹P{¹H} NMR (C₆D₆): δ = −63.0 (s) ppm; ²⁹Si{¹H} NMR (C₆D₆):

δ = −0.7 [d, ²*J*(P,Si) = 8.0 Hz], 1.6 [d, ²*J*(P,Si) = 9.1 Hz] ppm. UV/Vis (CH₂Cl₂): λ_{\max} (log ϵ) = 205.5 (0.41), 250.0 (3.91), 255.5 (4.00), 340.5 (0.59), 471.5 (0.13) nm. MS (EI, 70 eV, ¹⁸⁴W): *m/z* (%) = 593.3 (3) [M]⁺, 382.0 (8) [M-FcCN]⁺, 354.0 (30) [M-FcCN-CO]⁺, 298.0 (5) [M-FcCN-3CO]⁺, 270.0 (40) [M-FcCN-4CO]⁺, 211.0 (100) [FcCN]⁺, 121.0 (35) [FeCp]⁺, 73.1 (20) [Si(Me₃)₃]⁺; C₂₃H₂₈CrFeNO₅PSi₂ (593.46): calcd. C 46.56, H 4.94, N 2.37; found C 46.55, H 4.76, N 2.36.

[[2-Bis(trimethylsilyl)methyl]-3-ferrocenyl-2*H*-azaphosphirene-κP]-pentacarbonylmolybdenum(0)] (1b**):** Red solid; yield 0.91 g (1.53 mmol, 41%); m.p. 114–115 °C. ¹H NMR (C₆D₆): δ = 0.05 [s, 9 H, Si(CH₃)₃], 0.16 [s, 9 H, Si(CH₃)₃], 0.41 [d, ²*J*(P,H) = 4.5 Hz, 1 H, CH], 3.99 (s, 5 H, Fc-Cp^bH), 4.62 (m_c, 2 H, Fc-Cp^aH³⁺⁴), 4.85 (m_c, 2 H, Fc-Cp^aH²⁺⁵) ppm. ¹³C{¹H} NMR (C₆D₆): δ = −0.8 [d, ³*J*(P,C) = 3.2 Hz, Si(CH₃)₃], 0.0 [d, ³*J*(P,C) = 2.6 Hz, Si(CH₃)₃], 26.8 [d, ¹*J*(P,C) = 29.7 Hz, CH], 67.8 (s, Fc-Cp^aC¹), 68.3 (s, Fc-Cp^bCH), 70.2 (s, Fc-Cp^aC²⁺⁵H), 70.9 (s, Fc-Cp^aC³⁺⁴H), 189.4 [d, ¹⁺²*J*(P,C) = 2.6 Hz, P-C=N], 203.2 [d, ²*J*(P,C) = 11.6 Hz, CO_{cis}], 206.6 [d, ²*J*(P,C) = 36.8 Hz, CO_{trans}] ppm. ³¹P{¹H} NMR (C₆D₆): δ = −94.9 (s) ppm. ²⁹Si{¹H} NMR (C₆D₆): δ = −0.5 [d, ²*J*(P,Si) = 7.8 Hz], 1.8 [d, ²*J*(P,Si) = 8.5 Hz] ppm. MS (EI, 70 eV, ¹⁸⁴W): *m/z* (%) = 639.0 (8) [M]⁺, 428.0 (17) [M-FcCN]⁺, 400.0 (12) [M-FcCN-CO]⁺, 372.0 (12) [M-FcCN-2CO]⁺, 344.0 (8) [M-FcCN-3CO]⁺, 316.0 (4) [M-FcCN-4CO]⁺, 288.0 (5) [M-FcCN-5CO]⁺, 211.0 (100) [FcCN]⁺, 121.0 (38) [FeCp]⁺, 73.1 (13) [Si(Me₃)₃]⁺.

Synthesis of [[2-Bis(trimethylsilyl)methyl]-3,5-diferrocenyl-2*H*-1,4,2-diazaphosphole-κP]pentacarbonylchromium(0)] (3a**):** To a stirred solution of 2*H*-azaphosphirene complex **1a** (292 mg, 0.48 mmol) and cyanoferrocene (**3**) (101 mg, 0.48 mmol) in CH₂Cl₂ (2.0 mL) was added ferrocenium hexafluorophosphate (16 mg, 0.048 mmol, 0.10 equiv.), and the reaction mixture turned dark red. After 13 d [reaction monitoring by ³¹P{¹H} NMR spectroscopy], the solvent was removed, and the product was purified by column chromatography on ALOX (−20 °C, petroleum ether/Et₂O, 100:1).

Complex 3a: Purple solid, crystallized from Et₂O. ¹H NMR (C₆D₆): δ = −0.17 [s, 9 H, Si(CH₃)₃], 0.37 [s, 9 H, Si(CH₃)₃], 1.20 [d, ²*J*(P,H) = 5.3 Hz, 1 H, CH(SiMe₃)₂], 4.14 (s, 5 H, Fc-Cp^bH), 4.23 (s, 5 H, Fc-Cp^bH), 4.23 (m_c, 2 H, Fc¹-CpH^{3,4}), 4.28 (m_c, 2 H, Fc²-CpH^{3,4}), 4.98 (m_c, 1 H, Fc¹-CpH⁵), 5.08 (m_c, 1 H, Fc¹-CpH³), 5.17 (m_c, 1 H, Fc²-CpH⁵), 5.26 (m_c, 1 H, Fc²-CpH²) ppm. ¹³C{¹H} NMR (CDCl₃): δ = 1.7 [d, ³*J*(P,C) = 2.1 Hz, Si(CH₃)₃], 2.2 [d, ³*J*(P,C) = 1.9 Hz, Si(CH₃)₃], 22.4 [d, ¹*J*(P,C) = 8.4 Hz, CH(SiMe₃)₂], 68.2 (s, Fc²-CpC⁵H), 68.6 (s, Fc-CpCH), 68.8 (s, Fc¹-CpC²H), 69.3 (s, Fc¹-CpC^{3/4}H), 69.8 (s, Fc-CpCH), 69.9 (s, Fc²-CpC^{3/4}H), 70.6 (s, Fc¹-CpC^{3/4}H), 70.8 (s, Fc²-CpC²H), 71.3 (s, Fc²-CpC^{3/4}H), 75.7 (s, Fc¹-CpC⁵H), 76.2 (s, Fc²-CpC¹), 80.8 (s, Fc¹-CpC¹), 171.6 [d, ²⁺³*J*(P,C) = 6.8 Hz, PNC], 205.3 [d, ¹⁺⁴*J*(P,C) = 12.0 Hz, PCN], 215.5 [d, ²*J*(P,C) = 22.0 Hz, CO_{trans}], 219.9 [d, ²*J*(P,C) = 6.1 Hz, CO_{cis}] ppm. ²⁹Si{¹H} NMR (C₆D₆): δ = 0.7 [d, ²*J*(P,Si) = 8.5 Hz], 2.1 [d, ²*J*(P,Si) = 6.0 Hz] ppm. ³¹P{¹H} NMR (C₆D₆): δ = 159.4 [s, ²*J*(P,H) = 5.0 Hz] ppm. IR (KBr): $\tilde{\nu}$ = 2962.6 (w, CH₃/CH), 2925.3 (w, CH₃/CH), 2057.9 (m, sh, CO), 1980.1 (m, sh, CO), 1925.9 (s, CO), 1555.5 (m, CN), 1505.6 (w, CN) cm^{−1}. UV/Vis (*n*-pentane): λ_{\max} (abs.) = 536.0 (0.051), 415.0 (0.037), 296.0 (0.219), 216.0 (0.818) nm. MS (EI): *m/z* (%) = 804 ([M]⁺, 10), 664 ([M⁺ − 5CO], 70), 612 ([M⁺ − Cr(CO)₅], 40), 211 ([Fc-CN]⁺, 100).

Synthesis of [[2-Bis(trimethylsilyl)methyl]-3,5-diferrocenyl-2*H*-1,4,2-diazaphosphole-κP]pentacarbonyltungsten(0)] (3c**):** To a stirred solution of 2*H*-azaphosphirene complex **1c** (579 mg, 0.80 mmol) and cyanoferrocene (**3**) (189 mg, 0.90 mmol) in CH₂Cl₂ (4.8 mL) was added ferrocenium hexafluorophosphate (48 mg, 0.15 mmol,

0.18 equiv.), and the reaction mixture turned deep purple. After 2 h [reaction monitoring by $^{31}\text{P}\{^1\text{H}\}$ NMR spectroscopy], the solvent was removed, and the product was purified by column chromatography on silica (-15°C , petroleum ether/ Et_2O , 10:1).

Complex 3c: Purple solid, crystallized from Et_2O ; yield 493 mg (0.53 mmol, 66%); m.p. 174°C . ^1H NMR (C_6D_6): $\delta = -0.13$ [s_{sat} , $^2J(\text{Si},\text{H}) = 6.3$ Hz, 9 H, $\text{Si}(\text{CH}_3)_3$], 0.35 [s_{sat} , $^2J(\text{Si},\text{H}) = 6.3$ Hz, 9 H, $\text{Si}(\text{CH}_3)_3$], 1.29 [d, $^2J(\text{P},\text{H}) = 6.5$ Hz, 1 H, $\text{CH}(\text{SiMe}_3)_2$], 4.14 (s, 5 H, $\text{Fc-Cp}^b\text{H}$), 4.22 (s, 5 H, $\text{Fc-Cp}^b\text{H}$), 4.23 (m_c , 2 H, $\text{Fc}^3\text{-Cp}^a\text{H}^{3,4}$), 4.28 (m_c , 2 H, $\text{Fc}^5\text{-Cp}^a\text{H}^{3,4}$), 4.94 (m_c , 1 H, $\text{Fc}^3\text{-Cp}^a\text{H}^5$), 5.11 (m_c , 1 H, $\text{Fc}^3\text{-Cp}^a\text{H}^2$), 5.15 (m_c , 1 H, $\text{Fc}^5\text{-Cp}^a\text{H}^5$), 5.25 (m_c , 1 H, $\text{Fc}^5\text{-Cp}^a\text{H}^2$) ppm. $^{13}\text{C}\{^1\text{H}\}$ NMR (C_6D_6): $\delta = 2.9$ [d, $^3J(\text{P},\text{C}) = 2.3$ Hz, $\text{Si}(\text{CH}_3)_3$], 3.5 [d, $^3J(\text{P},\text{C}) = 2.3$ Hz, $\text{Si}(\text{CH}_3)_3$], 23.7 [d, $^1J(\text{P},\text{C}) = 5.2$ Hz, $\text{CH}(\text{SiMe}_3)_2$], 69.9 (s, $\text{Fc}^5\text{-Cp}^a\text{C}^5\text{H}$), 70.3 (s, $\text{Fc-Cp}^b\text{CH}$), 70.5 (s, $\text{Fc}^3\text{-Cp}^a\text{C}^2\text{H}$), 70.9 (s, $\text{Fc}^3\text{-Cp}^a\text{C}^{3/4}\text{H}$), 71.3 (s, $\text{Fc-Cp}^b\text{CH}$), 71.4 (s, $\text{Fc}^5\text{-Cp}^a\text{C}^{3/4}\text{H}$), 72.2 [d, $^4J(\text{P},\text{C}) = 1.0$ Hz, $\text{Fc}^3\text{-Cp}^a\text{C}^{3/4}\text{H}$], 72.3 [d, $^4J(\text{P},\text{C}) = 2.6$ Hz, $\text{Fc}^5\text{-Cp}^a\text{C}^2\text{H}$], 73.0 (s, $\text{Fc}^5\text{-Cp}^a\text{C}^{3/4}\text{H}$), 76.4 [d, $^3J(\text{P},\text{C}) = 1.9$ Hz, $\text{Fc}^3\text{-Cp}^a\text{C}^5\text{H}$], 77.7 [d, $^3J(\text{P},\text{C}) = 12.9$ Hz, $\text{Fc}^5\text{-Cp}^a\text{C}^1$], 81.4 [d, $^2J(\text{P},\text{C}) = 29.7$ Hz, $\text{Fc}^3\text{-Cp}^a\text{C}^1$], 175.1 [d, $^{2+3}J(\text{P},\text{C}) = 5.8$ Hz, PNC], 197.9 [d_{sat} , $^2J(\text{P},\text{C}) = 6.1$, $^1J(\text{W},\text{C}) = 126.4$ Hz, CO_{cis}], 198.6 [d, $^2J(\text{P},\text{C}) = 22.0$ Hz, CO_{trans}], 206.6 [d, $^{1+4}J(\text{P},\text{C}) = 27.5$ Hz, PCN] ppm. $^{29}\text{Si}\{^1\text{H}\}$ NMR (C_6D_6): $\delta = 1.1$ [d, $^2J(\text{P},\text{Si}) = 8.0$ Hz], 2.4 [d, $^2J(\text{P},\text{Si}) = 4.9$ Hz] ppm. $^{31}\text{P}\{^1\text{H}\}$ NMR (C_6D_6): $\delta = 114.4$ (d_{sat} , $^1J(\text{P},\text{W}) = 234.0$, $^2J(\text{P},\text{H}) = 6.5$ Hz) ppm. IR (KBr): $\tilde{\nu} = 2961.0$ (w, CH_3/CH), 2924.6 (w, CH_3/CH), 2900.1 (w, CH_3/CH), 2066.9 (m, sh, CO), 1978.6 (m, sh, CO), 1947.0 (s, CO), 1927.2 (s, CO), 1921.3 (s, CO), 1555.5 (m, CN), 1505.6 (w, CN) cm^{-1} . UV/Vis (*n*-pentane): λ_{max} (abs.) = 538.5 (0.055), 404.0 (0.054), 295.5 (0.209), 249.0 (0.614), 226.5 (0.955), 205.0 (1.143) nm. MS (FAB+, *m*NBA): *m/z* (%) = 935.9 ($[\text{M} + \text{H}]^+$, 11), 880 ($\text{M}^+ - 2\text{CO}$, 30), 796 ($\text{M}^+ - 5\text{CO}$, 10), 613 ($[\text{M} + \text{H} - \text{W}(\text{CO})_5]^+$, 85), 612.1 ($\text{M}^+ - \text{W}(\text{CO})_5$, 100); $\text{C}_{34}\text{H}_{37}\text{Fe}_2\text{N}_2\text{O}_5\text{PSi}_2\text{W}$ (936.34): calcd. C 43.61, H 3.98, N 2.99; found C 43.87, H 4.12, N 2.88.

Computational Details: Calculated geometries were fully optimized in the gas phase with tight convergence criteria at the DFT level with the Gaussian 03 package,^[46] by using the B3LYP^[47] functional and two different levels depending on the basis sets. In one of them (method A), the optimizations were carried out with the 6-31G* basis set for all atoms, adding diffuse functions on donor atoms (N and F) (denoted as aug6-31G*) as well as the LanL2DZ basis set, with effective core potential, for Cr, Mo, and W. From these gas-phase optimized geometries all reported data were obtained by means of single-point (SP) calculations. Energy values were computed with the aug6-311G**/LanL2DZecp basis set and by considering solvent (dichloromethane) effects by using Cossi and Barone's CPCM formalism^[20,21] and including the correction for the zero-point vibrational energy at the optimization level. The same basis sets were used to perform the Natural Bond Orbital (NBO) population analysis^[31] from which natural charges were obtained. Bond orders were characterized by the Wiberg bond index (WBI) and calculated with the NBO method as the sum of squares of the off-diagonal density matrix elements between atoms.^[48] Where explicitly stated (see the Supporting Information), a higher level of theory (method B) was used by employing the aug631G** basis set for both optimizations and SP calculations (energies and NBO analysis) for all atoms except Cr, Mo, and W, for which the Stuttgart relativistic small core basis set with effective core potential^[49] was employed. Topological analysis of the electronic charge density $\rho(r_c)$ and its Laplacian, $\nabla^2\rho(r_c)$, was performed by means of the AIM (atoms-in-molecules) theory of molecular structure proposed by Bader and coworkers,^[50] by using the wavefunction correspond-

ing to the optimization level of theory and the AIM2000 software.^[51]

Supporting Information (see also the footnote on the first page of this article): Study of the effect of the metal on the oxidation of acyclic, common phosphane complexes $[\text{M}(\text{CO})_5(\text{PR}_3)]$ (Figures S1 and S2). Effects of the substituent and the metal on the geometric changes of selected bonds upon oxidation of **3** (Figure S3).

Acknowledgments

We are grateful to the Deutsche Forschungsgemeinschaft (DFG), the Fonds der Chemischen Industrie (Kekulé Stipendium for H. H.), the Rheinische Friedrich-Wilhelms-Universität Bonn (SFB 624: "Templates – From Design Chemical Matrices to Reaction Control"), and the John von Neumann Institute for Computing. A. E. wishes to acknowledge the financial support from Fundación Séneca (Agencia de Ciencia y Tecnología de la Región de Murcia), projects 02970/PI/05 and 04509/GERM/06.

- [1] F. Palacios, A. M. Ochoa de Retana, E. Martínez de Mari-gorta, J. M. de los Santos, *Eur. J. Org. Chem.* **2001**, 2401–2414.
- [2] a) K. Dietliker, H. Heimgartner, *Helv. Chim. Acta* **1983**, *66*, 262–295; b) A. Demoulin, H. Gorissen, A.-M. Hesbain-Frisque, L. Ghosez, *J. Am. Chem. Soc.* **1975**, *97*, 4409–4410.
- [3] a) F. Müller, J. Mattay, *Angew. Chem.* **1991**, *103*, 1352–1337; *Angew. Chem. Int. Ed. Engl.* **1991**, *30*, 1336–1337; b) F. Müller, J. Mattay, *Chem. Rev.* **1993**, *93*, 99–117.
- [4] C. Gaebert, J. Mattay, M. Toubartz, S. Steenken, B. Müller, T. Bally, *Chem. Eur. J.* **2005**, *11*, 1294–1304.
- [5] F. Mathey (Ed.), *Phosphorus-Carbon Heterocyclic Chemistry: The Rise of a New Domain*, Pergamon, Oxford, **2001**.
- [6] a) K. B. Dillon, F. Mathey, J. F. Nixon, *Phosphorus: The Carbon Copy*, Wiley, New York, **1998**; b) Here, the observation was reported that this analogy becomes even more pronounced if the phosphorus atom is bonded to a pentacarbonyl-coordinated transition-metal center.
- [7] R. Streubel, *Coord. Chem. Rev.* **2002**, *227*, 175–192.
- [8] R. Streubel, *Top. Curr. Chem.* **2002**, *223*, 91–101.
- [9] a) R. Streubel, C. Neumann, P. G. Jones, *J. Chem. Soc., Dalton Trans.* **2000**, 2495–2496; b) C. Neumann, E. Ionescu, U. Schiemann, M. Schlenker, M. Bode, F. Ruthe, P. G. Jones, R. Streubel, *J. Organomet. Chem.* **2002**, *643–644*, 253–264; c) C. Neumann, A. Pehn Junquera, C. Wismach, P. G. Jones, R. Streubel, *Tetrahedron* **2003**, *59*, 6213–6220.
- [10] K. E. Torrance, L. McElwee-White, *Coord. Chem. Rev.* **2000**, *206–207*, 469–491.
- [11] H. Helten, C. Neumann, A. Espinosa, P. G. Jones, M. Nieger, R. Streubel, *Eur. J. Inorg. Chem.* **2007**, 4669–4678.
- [12] R. Streubel, M. Beckmann, C. Neumann, S. Fankel, H. Helten, O. Feier-Iova, P. G. Jones, M. Nieger, *Eur. J. Inorg. Chem.* **2009**, 2090–2095.
- [13] The $^{31}\text{P}\{^1\text{H}\}$ NMR spectroscopic data of complexes **4a–c** ratios **3a/4a** = 5:1, **3b/4b** = 13:1, and **3c/4c** = 15:1; the values **4a**: $\delta = 291.6$ [t, $^1J(\text{P},\text{F}) = 1091.0$ Hz] ppm, **4b**: $\delta = 266.5$ [t, $^1J(\text{P},\text{F}) = 1082.1$ Hz] ppm, **4c**: $\delta = 233.3$ [t, $^1J(\text{P},\text{F}) = 1068.1$, $^1J(\text{W},\text{P}) = 359.9$ Hz] ppm are very similar to those of the *P*-*t*Bu-substituted difluorophosphane complexes $[\text{M}(\text{CO})_5\{\text{PF}_2\text{tBu}\}]$ {M = Cr: $\delta = 285.5$ (t, $^1J(\text{P},\text{F}) = 1195$ Hz) ppm; M = Mo: $\delta = 262.2$ [t, $^1J(\text{P},\text{F}) = 1090$ Hz] ppm; M = W: $\delta = 235.1$ [t, $^1J(\text{P},\text{F}) = 1089$ Hz] ppm} presented in O. Stelzer, R. Schmutzler, *J. Chem. Soc. A* **1971**, 2867–2873.
- [14] From reaction (i), complex **3c** was obtained (with slight impurity) after low-temperature column chromatography, and its constitution was unambiguously confirmed by multinuclear (^1H , ^{13}C , ^{29}Si , ^{31}P) NMR spectroscopic experiments and mass spectrometry.

- [15] X-ray crystallographic analysis of **3a** and **3c**: suitable purple single crystals of **3a** and **3c** were obtained from concentrated Et₂O solution upon decreasing the temperature from ambient temperature to +4 °C. Data were collected with a Nonius KappaCCD diffractometer at 123 K by using graphite-monochromated Mo-K α radiation ($\lambda = 0.71073$ Å). The structures were solved by Patterson methods (**3c**) and direct methods (**3a**) (SHELXS-97)^[16] and refined by full-matrix least-squares on F^2 (SHELXL-97).^[16] All non-hydrogen atoms were refined anisotropically. The hydrogen atoms were included isotropically by using the riding model on the bound atoms. Semiempirical absorption corrections were carried out from equivalents [min./max. transmissions: 0.77507/0.81056 (for **3a**), 0.35828/0.47065 (for **3c**)]. C₃₄H₃₇CrFe₂N₂O₅PSi₂ (**3a**); crystal size 0.25 × 0.20 × 0.15 mm, monoclinic, $P2_1/c$ (No.14), $a = 18.1979(4)$ Å, $b = 10.2731(2)$ Å, $c = 19.8117(7)$ Å, $\beta = 107.337(1)^\circ$, $V = 3535.51(16)$ Å³, $Z = 4$, $\rho_{\text{calc}} = 1.511$ Mg m⁻³, $2\theta_{\text{max}} = 55^\circ$, collected (independent) reflections = 18739 (7903), $R_{\text{int}} = 0.0451$, $\mu = 1.268$ mm⁻¹, 424 refined parameters, 0 restraints, R_1 [for $I > 2\sigma(I)$] = 0.0331, wR_2 (for all data) = 0.0579, max./min. residual electron density: 0.371/-0.413 e Å⁻³. C₃₄H₃₇Fe₂N₂O₅PSi₂W (**3c**); crystal size 0.30 × 0.20 × 0.15 mm, monoclinic, $P2_1/c$ (No.14), $a = 18.2463(3)$ Å, $b = 10.3139(2)$ Å, $c = 19.9059(3)$ Å, $\beta = 106.247(1)^\circ$, $V = 3596.50(11)$ Å³, $Z = 4$, $\rho_{\text{calc}} = 1.729$ Mg m⁻³, $2\theta_{\text{max}} = 55^\circ$, collected (independent) reflections = 24244 (8139), $R_{\text{int}} = 0.0601$, $\mu = 4.140$ mm⁻¹, 424 refined parameters, 0 restraints, R_1 [for $I > 2\sigma(I)$] = 0.0326, wR_2 (for all data) = 0.0741, max./min. residual electron density: 1.385/-2.022 e Å⁻³. CCDC-713843 (for **3a**) and -713842 (for **3c**) contain the supplementary crystallographic data for this paper. These data can be obtained free of charge from The Cambridge Crystallographic Data Centre via www.ccdc.cam.ac.uk/data_request/cif.
- [16] G. M. Sheldrick, *Acta Crystallorg. Sect. A* **2008**, *64*, 112–122.
- [17] R. Streubel, H. Wilkens, F. Ruthe, P. G. Jones, *Tetrahedron* **2000**, *56*, 21–26.
- [18] The numbering of atoms in the heterocyclic complexes according to the Hantzsch–Widman–Patterson nomenclature is used in this paper.
- [19] J. Mason, *Multinuclear NMR*, Plenum Press, New York, **1987**.
- [20] a) V. Barone, M. Cossi, *J. Phys. Chem. A* **1998**, *102*, 1995–2001; b) M. Cossi, N. Rega, G. Scalmani, V. Barone, *J. Comput. Chem.* **2003**, *24*, 669–681.
- [21] a) S. Miertus, E. Scrocco, J. Tomasi, *J. Chem. Phys.* **1981**, *55*, 117–129; b) R. Cammi, B. Mennucci, J. Tomasi, *J. Phys. Chem. A* **2000**, *104*, 5631–5637.
- [22] Changing group R¹ from methyl to bis(silyl)methyl (for R² = Me, not shown in Figure 2) does not introduce significant differences, except for slightly favoring all three processes.
- [23] N. G. Connelly, W. E. Geiger, *Chem. Rev.* **1996**, *96*, 877–910.
- [24] a) V. Lloveras, A. Caballero, A. Tárraga, M. D. Velasco, A. Espinosa, K. Wurst, D. J. Evans, J. Vidal-Gancedo, C. Rovira, P. Molina, J. Veciana, *Eur. J. Inorg. Chem.* **2005**, 2436–2450; b) A. Caballero, A. Espinosa, A. Tárraga, P. Molina, *J. Org. Chem.* **2008**, *73*, 5489–5497.
- [25] Cp^a and Cp^b denote the monosubstituted and the unsubstituted cyclopentadienyl rings, respectively.
- [26] S. Lupan, M. Kapon, M. Cais, F. H. Herstein, *Angew. Chem.* **1972**, *84*, 1104–1106; *Angew. Chem. Int. Ed. Engl.* **1972**, *11*, 1025–1027.
- [27] R. F. W. Bader, *Atoms in Molecules: A Quantum Theory*, Oxford University Press, Oxford, **1990**.
- [28] These results follow a trend similar to that recently reported with regard to the influence of *N*-protonation on the strength (or better, stiffness) of relevant bonds in simple models of azaphosphiridine and 2*H*-azaphosphirenechromium(0) complexes by using the compliance constant method: H. Heltén, G. v. Frantzius, G. Schnakenburg, J. Daniels, R. Streubel, *Eur. J. Inorg. Chem.* **2009**, 2062–2065.
- [29] For instance see W. Nakanishi, T. Nakamoto, S. Hayashi, T. Sasamori, N. Tokitoh, *Chem. Eur. J.* **2007**, *13*, 255–268 and references cited therein.
- [30] M. J. S. Dewar, G. P. Ford, *J. Am. Chem. Soc.* **1979**, *101*, 783–791.
- [31] a) J. E. Carpenter, F. Weinhold, *THEOCHEM* **1988**, *169*, 41–62; b) J. E. Carpenter, Ph. D. Thesis, University of Wisconsin, Madison, WI, **1987**; c) J. P. Foster, F. Weinhold, *J. Am. Chem. Soc.* **1980**, *102*, 7211–7218; d) A. E. Reed, F. Weinhold, *J. Chem. Phys.* **1983**, *78*, 4066–4073; e) A. E. Reed, R. B. Weinstock, F. Weinhold, *J. Chem. Phys.* **1985**, *83*, 735–746; f) A. E. Reed, L. A. Curtiss, F. Weinhold, *Chem. Rev.* **1988**, *88*, 899–926.
- [32] α -SOMO orbital coefficients vary similarly for P (1.493), C (0.357), and N (0.380).
- [33] R. G. Parr, W. Yang, *Density Functional Theory of Atoms and Molecules*, Oxford University Press, Oxford, **1989**.
- [34] a) P. K. Chattaraj, H. Lee, R. G. Parr, *J. Am. Chem. Soc.* **1991**, *113*, 1855–1856; b) A. Cedillo, P. K. Chattaraj, R. G. Parr, *Int. J. Quantum Chem.* **2000**, *77*, 403–407.
- [35] R. G. Pearson, *J. Am. Chem. Soc.* **1963**, *85*, 3533–3539.
- [36] See for instance: A. Ponti, G. Molteni, *Chem. Eur. J.* **2006**, *12*, 1156–1161 and references cited therein.
- [37] R. G. Parr, W. Yang, *J. Am. Chem. Soc.* **1984**, *106*, 4049–4050.
- [38] a) S. Damoun, G. Van deWoude, F. Méndez, P. Geerlings, *J. Chem. Phys.* **1997**, *101*, 886–893; b) A. Ponti, *J. Phys. Chem. A* **2000**, *104*, 8843–8846.
- [39] A. Espinosa, A. Frontera, R. García, M. A. Soler, A. Tárraga, *Arkivoc* **2005**, *9*, 415–437.
- [40] R. G. Parr, L. V. Szentpaly, S. Liu, *J. Am. Chem. Soc.* **1999**, *121*, 1922–1924.
- [41] F. De Proft, W. Langenaeker, P. Geerlings, *J. Phys. Chem.* **1993**, *97*, 1826–1831; F. De Proft, S. Amira, K. Choho, P. Geerlings, *J. Phys. Chem.* **1994**, *98*, 5227–5233; S. Kishnamurthy, S. Pal, *J. Phys. Chem. A* **2000**, *104*, 7639–7645.
- [42] R. Parthasarathi, J. Padmanabhan, M. Elango, V. Subramanian, P. K. Chattaraj, *Chem. Phys. Lett.* **2004**, *394*, 225–230.
- [43] It is worth mentioning that the intermediate initially formed is not 9⁺ but a less stable rotamer that is easily converted into 9⁺ through an almost barrierless bond rotation process. Nevertheless, only the most stable conformer 9⁺ will be considered herein for the sake of simplicity.
- [44] Neither the unstable radical byproduct PF₄[•], nor its plausible stable disproportionation products PF₃ and PF₅ have ever been detected in our experiments. This latest disproportionation reaction could provide an extra driving force for the overall reaction sequence, as it has been estimated to be highly exergonic ($\Delta G^\circ = -31.2$ kJ mol⁻¹) at the working level of theory.
- [45] A. N. Nesmeyanov, E. G. Perevalova, L. P. Yuryeva, K. I. Grandberg, *Izv. Akad. Nauk SSSR, Ser. Khim.* **1962**, 1772–1777.
- [46] M. J. Frisch, G. W. Trucks, H. B. Schlegel, G. E. Scuseria, M. A. Robb, J. R. Cheeseman, J. A. Montgomery Jr, T. Vreven, K. N. Kudin, J. C. Burant, J. M. Millam, S. S. Iyengar, J. Tomasi, V. Barone, B. Mennucci, M. Cossi, G. Scalmani, N. Rega, G. A. Petersson, H. Nakatsuji, M. Hada, M. Ehara, K. Toyota, R. Fukuda, J. Hasegawa, M. Ishida, T. Nakajima, Y. Honda, O. Kitao, H. Nakai, M. Klene, X. Li, J. E. Knox, H. P. Hratchian, J. B. Cross, V. Bakken, C. Adamo, J. Jaramillo, R. Gomperts, R. E. Stratmann, O. Yazyev, A. J. Austin, R. Cammi, C. Pomelli, J. W. Ochterski, P. Y. Ayala, K. Morokuma, G. A. Voth, P. Salvador, J. J. Dannenberg, V. G. Zakrzewski, S. Dapprich, A. D. Daniels, M. C. Strain, O. Farkas, D. K. Malick, A. D. Rabuck, K. Raghavachari, J. B. Foresman, J. V. Ortiz, Q. Cui, A. G. Baboul, S. Clifford, J. Cioslowski, B. B. Stefanov, G. Liu, A. Liashenko, P. Piskorz, I. Komaromi, R. L. Martin, D. J. Fox, T. Keith, M. A. Al-Laham, C. Y. Peng, A. Nanayakkara, M. Challacombe, P. M. W. Gill, B. Johnson, W. Chen, M. W. Wong, C. Gonzalez, J. A. Pople, *Gaussian 03*, revision B.03, Gaussian, Inc., Wallingford CT, **2004**.

- [47] L. J. Bartolotti, K. Fluchick in *Reviews in Computational Chemistry* (Eds.: K. B. Lipkowitz, B. D. Boyd), VCH, Weinheim, **1996**, vol. 7, pp. 187–216.
- [48] K. Wiberg, *Tetrahedron* **1968**, *24*, 1083–1096.
- [49] The Stuttgart relativistic small core basis set was obtained from the Extensible Computational Chemistry Environment Basis Set Database, Version 10/29/02, as developed and distributed by the Molecular Science Computing Facility, Environmental and Molecular Sciences Laboratory, which is part of the Pacific Northwest Laboratory, P.O. Box 999, Richland, Washington 99352, USA and is funded by the U.S. Department of Energy. The Pacific Northwest Laboratory is a multiprogram laboratory operated by Battelle Memorial Institute for the U.S. Department of Energy under contract DE-AC06-76RLO 1830.
- [50] R. F. W. Bader, S. G. Anderson, A. J. Duke, *J. Am. Chem. Soc.* **1979**, *101*, 1389–1395; R. F. W. Bader, T. S. Slee, D. Cremer, E. Kraka, *J. Am. Chem. Soc.* **1983**, *105*, 5061–5068; R. F. W. Bader, P. J. MacDougall, *J. Am. Chem. Soc.* **1985**, *107*, 6788–6795; R. F. W. Bader, P. J. MacDougall, C. D. H. Lau, *J. Am. Chem. Soc.* **1984**, *106*, 1594–1605.
- [51] AIM2000 v. 2.0, designed by F. W. Biegler-König and J. Schönbohm, **2002**, <http://www.aim2000.de/>; F. Biegler-König, J. Schönbohm, D. Bayles, *J. Comput. Chem.* **2001**, *22*, 545–559; F. Biegler-König, J. Schönbohm, *J. Comput. Chem.* **2002**, *23*, 1489–1494.

Received: April 6, 2009
Published Online: July 1, 2009